Avalanche Photodiodes Based on the AlInAsSb Materials System

Seth R. Bank, *Senior Member, IEEE*, Joe C. Campbell, *Fellow, IEEE*, Scott J. Maddox, Min Ren, *Member, IEEE*, Ann-Katheryn Rockwell, Madison E. Woodson, and Stephen D. March

(Invited Paper)

***Abstract*—We report avalanche photodiodes (APDs) fabricated from high-aluminum-content $Al_xIn_{1-x}As_ySb_{1-y}$ lattice matched to GaSb that is grown within the miscibility gap using a digital alloy approach. The material was initially characterized through a series of $Al_xIn_{1-x}As_ySb_{1-y}$ ($x = 0.3, 0.4, 0.5, 0.6, 0.7$) p-i-n structures. In order to achieve operation at telecommunications wavelengths, an $Al_xIn_{1-x}As_ySb_{1-y}$ separate absorption, charge, and multiplication APD has been developed. Very low excess noise, as characterized by $k \sim 0.01-0.05$, has been achieved.**

***Index Terms*—InGaAs/InP, silicon, photodiode, photodetector.**

I. Introduction

OVER the past five decades avalanche photodiodes (APDs) have been utilized for a wide range of commercial, military, and research applications. Optical fiber communications has been one of the primary drivers for recent advances in APD performance, particularly structures and materials designed for low noise and high gain-bandwidth product in the short-wavelength infrared spectrum. The two most common photodetectors for optical receivers are p-i-n photodiodes and APDs. P-i-n photodiodes have the advantages of low bias, uncomplicated bias circuits without temperature control, and high reliability. APDs on the other hand, operate at 10's of volts bias, often require temperature stabilization, and are more susceptible to failure than p-i-n's. These disadvantages are offset by the potential for APDs to achieve higher receiver sensitivity, owing to their internal gain. The primary source of noise in a p-i-n photodiode is the shot noise of the dark and signal currents. This is typically less than that of the following circuitry. The shot noise of an APD is multiplied by the square of the average gain since the current increases linearly with gain; it can be expressed as [1].

$$\left\langle i_{shot}^2 \right\rangle = 2q(I_{photo} + I_{dark})\langle M \rangle^2 F(M)\Delta f \qquad (1)$$

where I_{photo} and I_{dark} are the photocurrent and dark current, respectively $<M>$ is the average value of the gain, and Δf is the bandwidth. Of particular importance is the excess noise factor, *F(M)*, which arises from the random nature of impact ionization. Not every carrier injected into the high-electric-field multiplication region gives rise to the same number of secondary ionizations. The resulting variation in gain is a source of additional noise represented by the excess noise factor, $F(M) = \langle M^2 \rangle / \langle M \rangle^2$. For bulk multiplication layers where non-local effects can be ignored, the excess noise factor is given by $F(M) = kM + (1 - k)\,[2 - 1/M]$, where k is the ratio of the electron, α, and hole, β, ionization coefficients such that by convention $k = \beta/\alpha$ if $\beta < \alpha$ and $k = \alpha/\beta$ if $\beta > \alpha$ [1]. The excess noise factor increases with increasing gain but increases more slowly the lower the value of *k*. The competition between the benefit of gain and its relationship to excess noise is illustrated by the signal to noise ratio, SNR,

$$SNR = \frac{I^2}{2qIF(M)\Delta f + \frac{\sigma^2}{M^2}} \qquad (2)$$

where $\sigma_{circuit}^2$ is the RMS noise current of the following amplifier. It is clear that until the gain becomes high enough for the excess noise to significantly affect the total noise, the APD gain effectively suppresses the amplifier noise. Thus, low excess noise, i.e., low *k*-values, are highly desirable in that they ultimately permit higher gain values and thus higher receiver sensitivity. It should be noted that low *k* values also yield high gain-bandwidth products [2].

First-generation optical fiber communication systems, operated in the wavelength range 800 nm to 900 nm, and utilized Si photodiodes [3] Si APDs exhibit very low excess noise, $k \sim 0.02$ [4], [5] and gain-bandwidth products >340 GHz [6].The long-wavelength cutoff of Si is $\sim 1.0\ \mu$m and the evolution of optical fiber communications to wavelengths in the range 1300 nm to 1600 nm lead to the development of InP-based APDs [7], [8].The highest receiver sensitivities were achieved with separate absorption, charge, and multiplication (SACM) structures consisting of an $In_{0.53}Ga_{0.47}As$ absorption region and an InP multiplication layer separated by an InP charge region to control the electric field profile [9]–[11]. The performance of these

Manuscript received May 24, 2017; revised July 25, 2017; accepted August 4, 2017. Date of publication August 11, 2017; date of current version August 25, 2017. This work was supported by the Army Research Office and DARPA under contract W911NF-10-1-0391. *(Corresponding author: Joe C. Campbell.)*

S. R. Bank and S. J. Maddox are with the Microelectronics Research Center, University of Texas, Austin, TX 78758 USA (e-mail:sbank@ece.utexas.edu; smaddox@utexas.edu).

J. C. Campbell, M. Ren, A.-K. Rockwell, M. E. Woodson, and S. D. March are with the Department of Electrical and Computer Engineering, University of Virginia, Charlottesville, VA 22904 USA (e-mail:jcc7s@virginia.edu; renmin1004@gmail.com; akrockwell@utexas.edu; mew2cc@virginia.edu; sdmarch@utmail.utexas.edu).

Color versions of one or more of the figures in this paper are available online at http://ieeexplore.ieee.org

Digital Object Identifier 10.1109/JSTQE.2017.2737880

APDs was limited by their relatively high k of ~0.45 and concomitant low gain-bandwidth product (<100 GHz). Lower excess noise has been achieved by designing thinner multiplication regions to take advantage of non-local effects and using $In_{0.52}Al_{0.48}As$ multiplication layers [12]–[14] Using this approach, recently, M. Nada *et al.*, have reported AlInAs/InGaAs APDs, for which the k value is ~0.2; these APDs achieved 235 GHz gain-bandwidth product and receiver sensitivity of −21 dBm at 25 Gb/s and 10^{-12} bit error rate [15] Another approach has been to combine a Ge absorption region with a Si multiplication layer in an SACM APD [6], [16]–[18]. In optical receivers, these APDs have achieved sensitivities as high as those of the best III-V compound APDs but not superior, as would have been expected from their low excess noise. This is due to the high dark current, that arises from the lattice mismatch between Ge and Si, which contributes enough to the noise to offset the lower excess noise factor. Recently, we have demonstrated APDs fabricated from $Al_xIn_{1-x}As_ySb_{1-y}$ digital alloys lattice-matched to GaSb [19], [20]. These APDs offer the advantages of III-V-compound direct-bandgap materials with high absorption coefficients and a lattice-matched material system that provides the flexibility to design complex structures to maximize performance and enable operation in different spectral regions. In addition, these APDs exhibit bulk excess noise comparable to Si. This paper reviews the design and performance of homojunction $Al_xIn_{1-x}As_ySb_{1-y}$ APDs with $x = 0.3$, 0.4, 0.5, 0.6, 0.7 and SACM structures that operate at telecomm wavelengths and exhibit excess noise characterized by $k = 0.01$.

II. Crystal Growth and Fabrication

Despite very recent progress in the growth of random alloys [21], lattice-matched $Al_xIn_{1-x}As_ySb_{1-y}$ on GaSb has seen only limited device application, due to the presence of a wide miscibility gap [22]–[24]. However, the groundbreaking work by Vaughn and co-workers [25]–[27] showed that AlInAsSb could be grown within the miscibility gap as a digital alloy of the constituent binaries, AlAs, AlSb, InAs, and InSb. As described in Ref. [28], we recently extended this method to cover the entire direct bandgap range of compositions using molecular beam epitaxy. This earlier work focused on spanning the compositional range with a fixed digital alloy period of 10 monolayers (ML); however, excellent material quality can also be achieved over a wide range of period thicknesses. Illustrative atomic force microscopy (AFM), bright-field transmission electron microscopy (TEM), and (224) X-ray diffraction (XRD) reciprocal space maps are shown in Fig. 1 for 300 nm-thick $Al_{0.5}In_{0.5}As_{0.5}Sb_{0.5}$ films grown with a 20 ML period. The RMS surface roughness was ~0.25 nm, consistent with the smooth and well-defined interfaces observed with TEM. Indeed, distinct superlattice fringes were observed both in ω-2θ XRD scans, as well as under reciprocal space mapping around the (224) GaSb reflection, consistent with excellent structural quality.

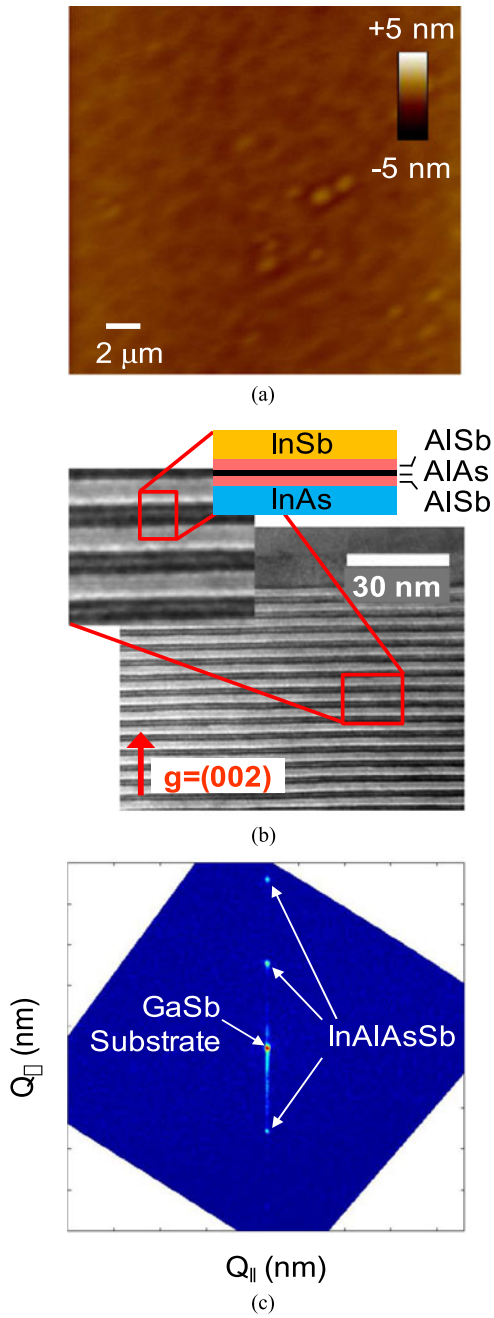

Fig. 1. Representative structural characteristics of AlInAsSb digital alloys illustrating the smooth morphology and well-defined interfaces. (a) Large-area atomic force microscopy, (b) bright-field transmission electron microscopy, and (c) (224) reciprocal space map for a 300 nm-thick $Al_{0.5}In_{0.5}As_{0.5}Sb_{0.5}$ film. RMS roughness was ~0.25 nm.

III. AlInAsSb/GaSb APDs

A cross-sectional schematic of the $Al_xIn_{1-x}As_ySb_{1-y}$/GaSb APDs is shown in Fig. 2. The growth sequence on the n^+ GaSb substrate consists of a 200 nm-thick n-type ($\sim 10^{18}$ cm^{-3}) GaSb layer, the unintentionally doped $Al_xIn_{1-x}As_ySb_{1-y}$ multiplication layer, 100 nm p -type (2×10^{18} cm^{-3}) $Al_xIn_{1-x}As_ySb_{1-y}$, and a thin (~30 nm) GaSb p-contact layer. The thickness of the unintentionally doped high-field multiplication region was 890 nm.

In the following, the wafers with $x = 0.7$ to 0.3 will simply be referred by the Al column III percentage, i.e., 70% to 30%. Fig. 3 shows dark currents versus bias voltage for 100 μm-diameter $Al_xIn_{1-x}As_ySb_{1-y}$/GaSb APDs at 300 K. The wider bandgap 70% and 60% samples exhibit the lowest dark current

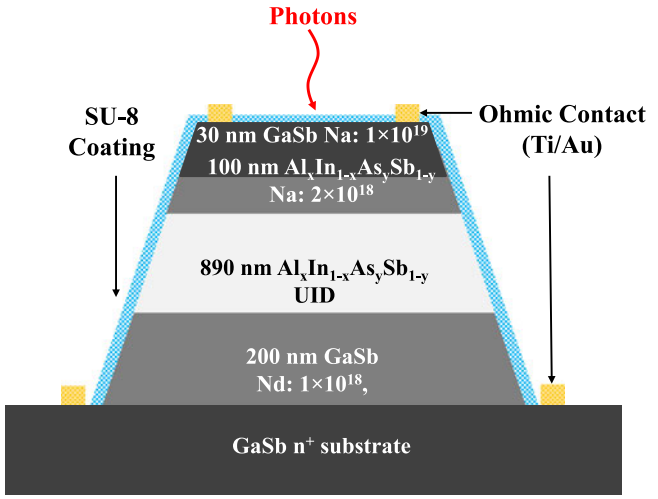

Fig. 2. Cross-sectional schematic of $Al_xIn_{1-x}As_ySb_{1-y}$ / GaSb p-i-n APDs.

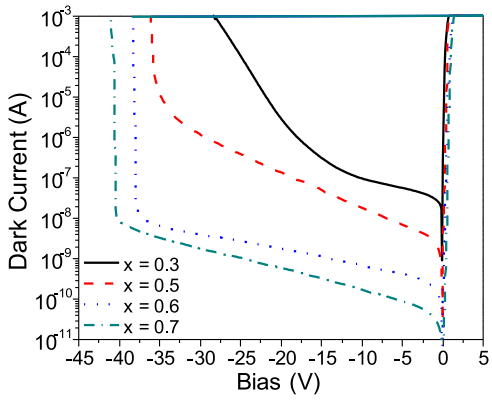

Fig. 3. Dark currents versus bias voltage of 50-μm-diameter $Al_xIn_{1-x}As_ySb_{1-y}$/GaSb APDs.

TABLE I
ACTIVATION ENERGIES EXTRACTED FROM TEMPERATURE-DEPENDENCE STUDY OF $Al_xIn_{1-x}As_ySb_{1-y}$/GaSb APDs

A $l_xIn_{1-x}As_ySb_{1-y}$ APDs, x =	0.3	0.4	0.5	0.6	0.7
Bias at measurement (V)	−25	−25	−30	−35	−35
Associated temperature range (K)	130 ∼ 190	130 ∼ 210	130 ∼ 210	130 ∼ 190	130 ∼ 190
Activation energy (eV)	0.06	0.06	0.05	0.06	0.1
Associated temperature range (K)	210 ∼ 270	230 ∼ 270	230 ∼ 270	210 ∼ 270	210 ∼ 270
Activation energy (eV)	0.11	0.13	0.1	0.32	0.32

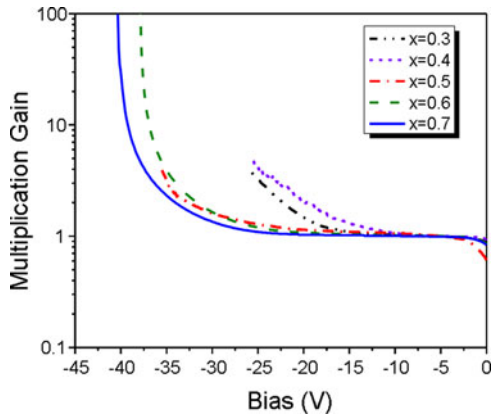

Fig. 4. Avalanche multiplication and measured photocurrents of $Al_xIn_{1-x}As_ySb_{1-y}$/GaSb APDs.

with well-defined breakdown voltages. Measurements of the dark current versus device diameter indicate that for the 60% devices the bulk and surface dark currents are comparable and that surface leakage dominates the 70% devices. The 30% and 50% devices exhibit much higher dark current that appears to originate in the bulk. This may reflect a combination of lower bandgap and poorer crystalline quality.

Temperature-dependence measurements were carried out from 130 K to 270 K. The temperature variation of the dark current can be expressed as [29].

$$I_{dN} \propto T^2 \exp\left(\frac{-E_a}{k_B T}\right) \tag{3}$$

where k_B is the Boltzmann constant and E_a is the activation energy. By fitting the measured dark current versus temperature, the activation energies for the $Al_xIn_{1-x}As_ySb_{1-y}$/GaSb wafers were estimated. In general, the dark current is characterized by more than one activation energy. However, since the APDs are typically operated at relatively high bias, the associated high-bias activation energies are summarized in Table I. When the temperature is lower than 200 K, a generation-recombination center with low activation energy is the dominant level in all the $Al_xIn_{1-x}As_ySb_{1-y}$/GaSb APDs. At higher temperatures, deeper generation-recombination centers are observed.

Capacitance-voltage measurements showed that the capacitances were relatively independent of voltage beyond −5 V, an indication that the unintentionally doped layers are fully depleted. It follows that the electric field is confined to that layer. A 543-nm He-Ne CW laser was used to measure photocurrent and extract multiplication gain. Once the bias voltage reaches −5 V, the photocurrents remain relatively flat until the field is sufficient for impact ionization. Accordingly, the unity gain point was set at −5 V for all compositions. Multiplication gains versus bias voltage are shown in Fig. 4. Gain as high as 100 was achieved in the x = 0.6 and 0.7 APDs. The gain in the x = 0.3, 0.4 and 0.5 APDs was lower and relatively unstable, due to the high dark current.

In Fig. 5 external quantum efficiencies at – 5 V bias are plotted versus wavelength. Measurements were taken using a tungsten-halogen light source, a monochrometer, and a lock-in amplifier. The photocurrents were referenced to calibrated silicon and InGaAs photodiodes. The collection of electrons created by absorption in the GaSb top contact layer is poor, especially

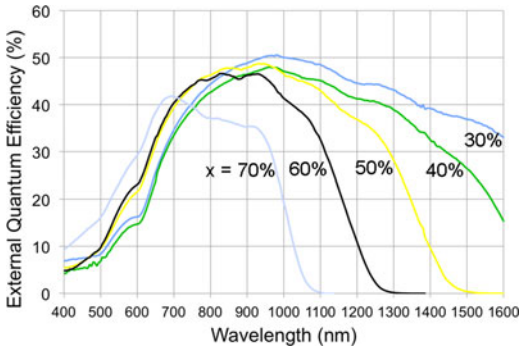

Fig. 5. External quantum efficiency of $Al_xIn_{1-x}As_ySb_{1-y}$/GaSb without GaSb top layer. All measurements were carried out with 200-μm diameter APDs at 300 K.

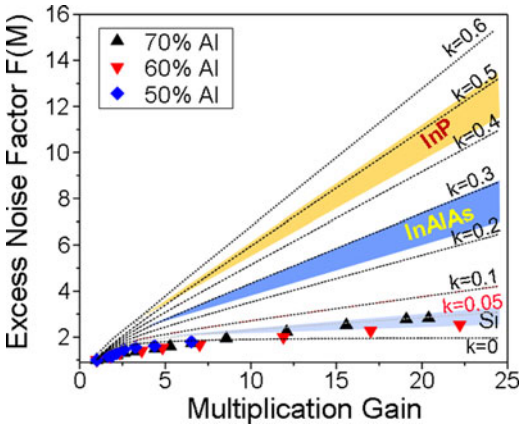

Fig. 6. Excess noise factor versus multiplication gain. The ▲, ▼, and ♢ symbols represent the excess noise factor of x = 0.7, 0.6 and 0.5 $Al_xIn_{1-x}As_ySb_{1-y}$/GaSb APDs, respectively. Typical excess noise of InP, InAlAs and Si are shown by shaded region.

for shorter wavelengths, due to surface recombination and a barrier at the GaSb/$Al_xIn_{1-x}As_ySb_{1-y}$ interface. Therefore, the GaSb top contact layer was removed using AZ 300 MIF except under the p-type contacts. The long-wavelength cutoff shifts with decreasing bandgap from ~1000 nm to >1600 nm as the Al fraction decreases from 70% to 30%. Note that these devices do not have anti-reflection coating and the absorption region is only ~1 μm thick.

The excess noise was measured with an HP 8970 noise figure meter and a 543-nm He-Ne CW laser. Fig. 6 shows F(M) versus gain. The solid lines are plots of the excess noise for *k*-values from 0 to 0.6 using the local-field model [1]. The k values for commercial Si APDs fall between 0.02 and 0.06; InP typically exhibits k values between 0.4 and 0.5; and InAlAs is in the range 0.2 and 0.3, as denoted by the shaded regions in Fig. 6. The x = 0.5, 0.6, and 0.7 APDs have *k* values as low as 0.01, which is comparable to that of Si APDs. The excess noise was only measured to gain values up to ~20. For higher gain the measurement apparatus became unstable owing to its dark current limit. Preliminary results suggest that the low hole ionization coefficient, β, can be attributed to high phonon scattering rates and the heavy effective hole mass [19], [20]. High

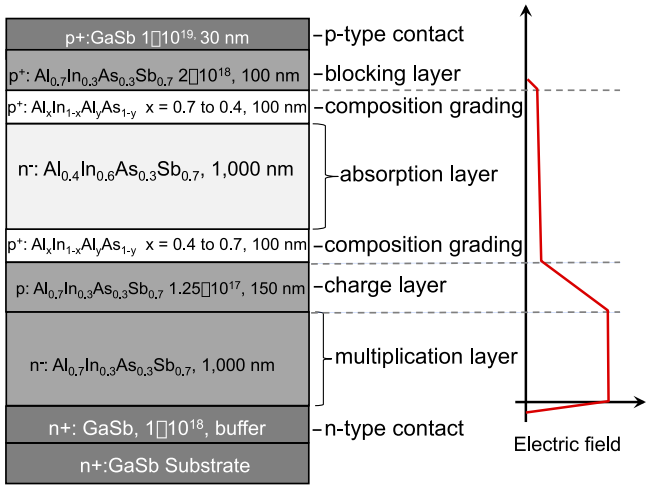

Fig. 7. Schematic cross section and electric field profile of $Al_xIn_{1-x}As_ySb_{1-y}$ SACM APD.

dark current prevented measurement of the excess noise of the x = 0.3 0.4 APDs.

IV. AlInAsSb SACM APDs

Figs. 3 and 5 illustrate the difficulty in fabricating homojunction $Al_xIn_{1-x}As_ySb_{1-y}$ APDs that operate at telecommunication wavelengths. Only the 30% and 40% samples exhibit photoresponse at 1550 nm and their dark current obviates operation at the high voltages required for significant impact ionization. The solution is to use a lower Al content layer for absorption and 60% or 70% Al for the multiplication region. Further, given the high dark current of the low Al material a charge layer is needed to maintain high field in the multiplication layer and low field in the absorber is beneficial. Fig. 7 is a cross sectional schematic of the $Al_{0.7}In_{0.3}As_{0.3}Sb_{0.7}/Al_{0.4}In_{0.6}As_{0.3}Sb_{0.7}$ SACM APD. In order to reduce charge accumulation at the heterojunction interfaces, 100 nm-thick compositionally graded layers (x = 0.4 to 0.7) are positioned on each side of the absorption layer.

A Monte-Carlo simulation, based on that in Refs. [30], [31], was employed to study the multiplication characteristics. The impact ionization rate, P_{ii}, was calculated using the Keldysh formula [32].

$$P_{ii} = \begin{cases} 0, & \text{if} \quad E < E_{th} \\ C_{ii}\left(\frac{E}{E_{th}} - 1\right)^r, & \text{if} \quad E \geq E_{th} \end{cases} \tag{4}$$

The phonon scattering rate, C_{ii}, and threshold energy, E_{th}, are treated as fitting parameters. Some important model parameters are listed in Table II.

The dark current, photocurrent, and gain versus bias voltage of a 50 μm-diameter SACM APD are shown in Fig. 8. The dark current at 95% breakdown is ~120 nA, which is approximately 100x lower than that of Ge on Si APDs [6], [16]–[18] and comparable to that of AlInAs/InGaAs APDs [15], [33], [34]. The gain is plotted on the right vertical axis. Gain values as high as 50 have been observed. The measured gain is well fit by the Monte

TABLE II
PARAMETERS USED IN MONTE-CARLO SIMULATION

Simulation Parameters	Electron	Hole
effective mass (m^*/m^0)	0.071	0.35
C_{ii}	8.0×10^{14}	8.0×10^{12}
r	3	3
E_{th}	2	10
Static dielectric constant	15.5	
High frequency dielectric constant	13.7	
Acoustic wave velocity (m/s)	2950	
Acoustic phonon energy (eV)	0.011	
Optical phonon energy (eV)	0.024	
Intervalley phonon energy (eV)	0.013	

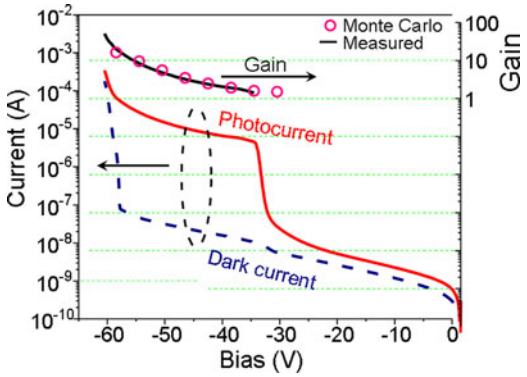

Fig. 8. Dark current, photocurrent, and measured and simulated (○) gain versus reverse bias of a 50-μm-diameter $Al_xIn_{1-x}As_ySb_{1-y}$ SACM APD at 300 K.

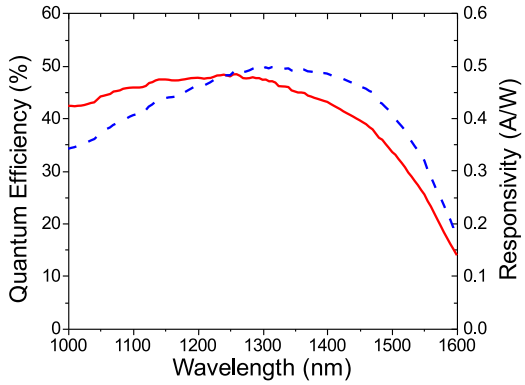

Fig. 9. External quantum efficiency and responsivity versus wavelength of a 150-μm-diameter $Al_xIn_{1-x}As_ySb_{1-y}$ SACM APD at 300 K.

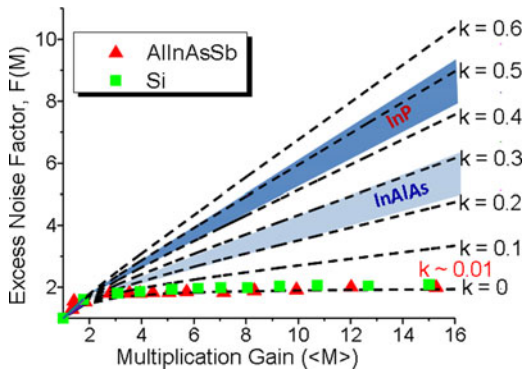

Fig. 10. Measured excess noise factor versus gain a 50-μm-diameter $Al_xIn_{1-x}As_ySb_{1-y}$ SACM APD (▲) and a comercial Si APD (■). The dashed lines are plots of the excess noise factor using the local field model for k values.

Carlo simulation. The step in the photocurrent near -38 V occurs when the edge of the depletion region reaches the absorbing layer, which is referred to as punch-through. The dark current scales with perimeter, which indicates that surface leakage dominates the dark current. Using the temperature-dependence of the dark current in Eq. (3) the activation energy was found to be 0.29 Ev $\pm$ 0.01 eV, which is approximately half the band-gap of $Al_{0.4}In_{0.6}As_{0.6}Sb_{0.4}$. This indicates that the dark current is primarily generated in the absorption layer through mid-bandgap states.

Owing to the high field in the multiplication layer, there is a small level of impact ionization at punch-through. By fitting the excess noise using the algorithm reported by H.-D. Liu *et al.* [35] the gain at punch-through was determined to be 1.7. This fit was confirmed by comparing responsivities with an $Al_{0.4}In_{0.6}As_{0.6}Sb_{0.4}$ control p-i-n photodiode, which has exactly the same 1000 nm absorption layer as the SACM APDs. This is also consistent with measurements of the gain in an $Al_{0.7}In_{0.3}As_{0.3}Sb_{0.7}$ homojunction APD at the same electric field as that of the SACM APD at punch-through [12]. As shown in Fig. 9, the optical cutoff wavelength is >1.6 μm. Note that the absorption layer is only 1,000 nm thick. Higher quantum efficiency, particularly at longer wavelengths, can be achieved with thicker absorption layers and by adding an anti-reflection coating to the top surface. Based on measurements of the absorption in 40% AlInAsSb homojunctions, we estimate the absorption coefficient at 1.55 μm to be $\sim 0.6 \times 10^4$ cm^{-1}. We a very good anti-reflection coating the quantum efficiency at 1.55 μm could exceed 80% with a 3 μm-thick absorption layer.

Fig. 10 shows the excess noise fig, F(M), versus the multiplication gain, for both the $Al_xIn_{1-x}As_ySb_{1-y}$ SACM APD (▲) and a commercial Si APD (■). The solid lines are plots of the excess noise for k-values from 0 to 0.6 using the local-field model. The measured $Al_xIn_{1-x}As_ySb_{1-y}$ SACM APD excess noise corresponds to an estimated *k*-value of 0.01, which is comparable to or less than that of Si [36], [37].

V. CONCLUSION

We have shown that high-performance avalanche photodiodes can be fabricated from the $Al_xIn_{1-x}As_ySb_{1-y}$ material system. Homojunction APDs having Al concentration from $x = 0.5$ to $x = 0.7$ exhibit low excess noise corresponding to $k = 0.01 \sim 0.05$ with peak quantum efficiencies of $\geq 50\%$ for absorption layers only 1 μm thick. The long-wavelength absorption of the low Al content quaternary was combined with the excellent avalanche characteristics of 70% material in an SACM APD. Operation was achieved in the telecommunications spectral window with excess noise characterized by $k = 0.01$. The $Al_xIn_{1-x}As_ySb_{1-y}$ materials have the potential for operation across a very wide wavelength range. By selecting suitable Al concentration or combining them one can build high performance photodetectors for a wide range of applications.

ACKNOWLEDGMENT

The authors acknowledge Minjoo Larry Lee and Daehwan Jung for performing the TEM studies.

REFERENCES

[1] R. J. McIntyre, "Multiplication noise in uniform avalanche diodes" *IEEE Trans. Electron Devices*, vol. ED-1, no. 1, pp. 164–168, Jan. 1966.
[2] R. B. Emmons, "Avalanche-photodiode frequency response," *J. Appl. Phys.*, vol. 38, pp. 3705–3714, 1967.
[3] H. Melchior, A. R. Hartman, D. P. Schinke, and T. E. Seidel, "Planar epitaxial silicon avalanche photodiode," *Bell Syst. Tech. J.*, vol. 57, pp. 1791–1807, 1978.
[4] C. A. Lee, R. A. Logan, R. L. Batdorf, J. J. Kleimack, and W. Weigmann, "Ionization rates of holes and electrons in silicon," *Phys. Rev.*, vol. 134, pp. A761–A773, 1964.
[5] J. Conradi, "The distributions of gains in uniformly multiplying avalanche photodiodes: Experimental," *IEEE Trans. Electron Devices*, vol. ED-19, no. 6, pp. 713–718, Jun. 1972.
[6] Y. Kang *et al.*, "Monolithic germanium/silicon avalanche photodiodes with 340 GHz gain-bandwidth product," *Nature Photon.*, vol. 3, pp. 59–63, 2009.
[7] J. C. Campbell, "Advances in photodetectors," in *Optical Fiber Telecommunications V Part A: Components and Subsystems*, I. P. Kaminow, T. Li, A. E. Willner, Eds., 5th ed. New York, NY, USA: Academic, 2008.
[8] J. C. Campbell, "Recent advances in avalanche photodiodes," *J. Lightw. Technol.*, vol. 34, no. 2, pp. 278–285, Jan. 2016.
[9] W. R. Clark *et al.*, "Reliable, high gain-bandwidth product InGaAs/InP avalanche photodiodes for 10 Gb/s receivers," in *Proc. Conf. Opt. Fiber Commun. Tech. Dig. Ser.*, 1999, pp. 1–3.
[10] D. S. G. Ong, M. M. Hayat, J. P. R. David, and J. S. Ng, "Sensitivity of high-speed lightwave system receivers using InAlAs avalanche photodiodes," *IEEE Photon. Technol. Lett.*, vol. 23, no. 4, pp. 233–235, Feb. 2011.
[11] M. A. Itzler, K. K. Loi, S. McCoy, N. Codd, and N. Komba, "High-performance, manufacturable avalanche photodiodes for 10 Gb/s optical receivers," in *Proc. Conf. Opt. Fiber Commun. Tech. Dig. Ser.*, vol. 4, 2000, pp. 126–128.
[12] E. Yagyu *et al.*, "Design and characteristics of guardring-free planar AlInAs avalanche photodiodes," *J. Lightw. Technol.*, vol. 27, no. 8, pp. 1011–1017, Apr. 2009.
[13] T. Nakata, T. Takeuchi, K. Makita, and T. Torikai, "High-speed and high-sensitivity waveguide InAlAs avalanche photodiodes for 10-40 Gb/s receivers," in *Proc. Conf. Proc. Lasers Electro-Opt. Soc. Annu. Meeting*, vol. 2, 2001, pp. 770–771.
[14] B. F. Levine *et al.*, "A new planar InGaAs-InAlAs avalanche photodiode," *IEEE Photon. Technol. Lett.*, vol. 18, no. 18, pp. 1898–1900, Sep. 2006.
[15] M. Nada, Y. Muramoto, H. Yokoyama, T. Ishibashi, and H. Matsuzaki, "Triple-mesa avalanche photodiode with inverted P-down structure for reliability and stability," *J. Lightw. Technol.*, vol. 32, no. 8, pp. 1543–1548, Apr. 2014.
[16] Y. Kang *et al.*, "High performance Ge/Si avalanche photodiodes development in Intel," in *Proc. 2011 Conf. Opt. Fiber Commun.*, 2011, pp. 1–3.
[17] N. Duan, T. Liow, A. Lim, L. Ding, and G. Q. Lo, "310 GHz gain-bandwidth product Ge/Si avalanche photodetector for 1550 nm light detection," *Opt. Express*, vol. 20, no. 10, pp. 11031–11036, May 2012.
[18] M. Huang *et al.*, "Development of Si photonics technology: Ge/Si avalanche photodiode for PON applications," in *Proc. Opt. Fiber Commun. Conf.*, 2014, Paper Tu2C.2.
[19] M. E. Woodson *et al.*, "Low-noise AlInAsSb avalanche photodiode," *Appl. Phys. Lett.*, vol. 108, no. 8, 2016, Art. no. 081102.
[20] M. Ren *et al.*, "AlInAsSb separate absorption, charge, and multiplication avalanche photodiodes," *Appl. Phys. Lett.*, vol. 108, no. 19, 2016, Art. no. 191108.
[21] J. Tournet, Y. Rouillard, and E. Tournié, "Growth and characterization of AlInAsSb layers lattice-matched to GaSb," *J. Cryst. Growth*, 2017, to be published.
[22] K. Onabe, "Immiscibility analysis for III-V quaternary solid solutions," *NEC Res. Dev.*, vol. 53, pp. 802–808, 1984.
[23] G. W. Turner, M. J. Manfra, H. K. Choi, and M.K. Connors, "MBE growth of high-power InAsSbInAlAsSb quantum-well diode lasers emitting at 3.5 μm," *J. Cryst. Growth*, vol. 175–176, pp. 825–832, May 1997.
[24] A. N. Semenov *et al.*, "Molecular beam epitaxy of AlInAsSb alloys near the miscibility gap boundary," *J. Cryst. Growth*, vol. 278, no. 2, pp. 203–2008, May 2005.
[25] L. G. Vaughn *et al.*, "Characterization of AlInAsSb and AlGaInAsSb MBE-grown digital alloys," in *Proc. Mater. Res. Soc. Symp.*, vol. 744, 2003, pp. M7.2.1–M7.2.12.
[26] L. G. Vaughn *et al.*, "Type-I mid-infrared MQW lasers using AlInAsSb barriers and InAsSb wells," *Proc. SPIE Phys. Simul. Optoelectron. Devices XIII*, vol. 5722, pp. 307–318, Apr. 2005.
[27] L. G. Vaughn, "Mid-infrared multiple quantum well lasers using digitally-grown alu- minum indium arsenic antimonide barriers and strained indium arsenic antimonide wells," Ph.D. dissertation, Univ. New Mexico, Albuquerque, NM, USA, 2006.
[28] S. J. Maddox, S. D. March, and S. R. Bank, "Broadly tunable AlInAsSb digital alloys grown on GaSb," *ACS Cryst. Growth Des.*, vol. 16, no. 7, pp. 3582–3586, Jun. 2016.
[29] W. Sun *et al.*, "High-gain InAs avalanche photodiodes" *IEEE J. Quantum Electron.*, vol. 49, no. 2, pp. 154–161, Feb. 2013.
[30] F. Ma *et al.*, "Monte carlo simulation of low-noise avalanche photodiodes with heterojunctions," *J. Appl. Phys.*, vol. 92, no. 8, pp. 4791–4795, 2002.
[31] W. Sun, X. Zheng, Z. Lu, and J. C. Campbell, "Monte carlo simulation of InAlAs/InAlGaAs tandem avalanche photodiodes," *J. Quantum Electron.*, vol. 48, no. 4, pp. 528–532, 2012.
[32] L. V. Keldysh, "Kinetic theory of impact ionization in semiconductors," *JETP Sov. Phys.*, vol. 37, no. 10, pp. 509–518, 1960.
[33] M. Nada, Y. Muramoto, H. Yokiyama, N. Ishibashi, and S. Kodama, "Inverted InAIAs/InGaAs avalanche photodiode with low-high-low electric field profile," *Jpn. J. Appl. Phys.*, vol. 51, no. 2, Feb. 2012, Art. no. 02BG03.
[34] M. Nada, Y. Muramoto, H. Yokoyama, T. Toshimatsu, and H. Matsuzaki, "High-speed avalanche photodiodes for 100-Gb/s systems and beyond," in *Proc. 2014 Eur. Conf. Opt. Commun.*, 2014, pp. 1–3.
[35] Han-Din Liu *et al.*, "Avalanche photodiode punch-through gain determination through excess noise analysis," *J. Appl. Phys.*, vol. 106, no. 6, Sep. 2009, Art. no. 064507.
[36] P. P. Webb, R. J. McIntyre, and J. Conradi, "Properties of avalanche photodiodes," *RCA Rev.*, vol. 35, no. 2, pp. 234–278, 1974.
[37] V. M. Robbins, T. Wang, K. F. Brennan, K. Hess, and G. E. Stillman, "Electron and hole impact ionization coefficients in (100) and in (111) Si," *J. Appl. Phys.*, vol. 58, pp. 4614–4617, 1985.

Seth R. Bank (S'95–M'06–SM'11) received the B.S. degree from the University of Illinois at Urbana-Champaign (UIUC), Urbana, IL, USA, in 1999, and the M.S. and Ph.D. degrees in 2003 and 2006, respectively, from Stanford University, Stanford, CA, USA, all in electrical engineering. While at UIUC, he studied the fabrication of InGaP–GaAs and InGaAs–InP HBTs. His Ph.D. research focused on the molecular beam epitaxy (MBE) growth, fabrication, and device physics of long-wavelength vertical-cavity surface-emitting lasers and low-threshold edge-emitting lasers in the GaInNAs(Sb)–GaAs material system. In 2006, he was a post-Doctoral Scholar with the University of California, Santa Barbara, CA, where his research centered on the growth of metal–semiconductor hetero- and nanostructures (e.g., ErAs nanoparticles in GaAs). In 2007, he joined the University of Texas at Austin, Austin, TX, USA, where he is currently an Associate Professor of Electrical and Computer Engineering and holder of the fifth Temple Foundation Endowed Faculty Fellowship. He has coauthored more than 175 papers and presentations in these areas. His current research interests include the MBE growth of novel heterostructures and nanocomposites and their device applications. He received a 2010 Young Investigator Program Award from ONR, a 2010 NSF CAREER Award, a 2009 Presidential Early Career Award for Scientists and Engineers nominated by ARO, a 2009 Young Investigator Program Award from AFOSR, the 2009 Young Scientist Award from the International Symposium on Compound Semiconductors, a 2008 DARPA Young Faculty Award, the 2008 Young Investigator Award from the North American MBE Meeting, and several best paper awards.

Joe C. Campbell (S'73–M'74–SM'88–F'90) received the B.S. degree from the University of Texas at Austin, Austin, TX, USA, in 1969, and the M.S. and Ph.D. degrees from the University of Illinois at Urbana-Champaign, Urbana, IL, USA, in 1971 and 1973, respectively, all in physics. From 1974 to 1976, he was with Texas Instruments, where he worked on integrated optics. In 1976, he joined the staff of AT&T Bell Laboratories, Holmdel, NJ. In the Crawford Hill Laboratory, he worked on a variety of optoelectronic devices including semiconductor lasers, optical modulators, waveguide switches, photonic integrated circuits, and photodetectors with emphasis on high-speed avalanche photodiodes for high-bit-rate lightwave systems. In January of 1989, he joined the faculty of the University of Texas at Austin as a Professor of Electrical and Computer Engineering and Cockrell Family Regents Chair in Engineering. In January of 2006, he became a member of the faculty at the University of Virginia, Charlottesville, VA, USA, as the Lucian Carr, III Chair of Electrical Engineering and Applied Science. To date, he has coauthored ten book chapters, 400 articles for refereed technical journals, and more than 400 conference presentations. His research has focused on the optoelectronic components that are used to generate, modulate, and detect the optical signals. At present, he is actively involved in single-photon-counting avalanche photodiodes, Si-based optoelectronics, high-speed, low-noise avalanche photodiodes, ultraviolet photodetectors, and quantum-dot IR imaging. He is a member of the National Academy of Engineering.

Scott J. Maddox received the B.S., M.S., and Ph.D. degrees from the University of Texas at Austin, Austin, TX, USA, in 2009, 2011, and 2015, respectively, where his research focused on the molecular beam epitaxial growth and characterization of novel III–V materials and optoelectronic devices including epitaxial plasmonic materials, dilute-bismuthide alloys for photodetector applications, and low-noise InAs and AlInAsSb avalanche photodiodes. In 2016, he joined Intel's Portland Technology Development Group, where he currently applies his knowledge of semiconductor growth, materials, and devices to develop the next generation of CMOS process nodes and help push the boundaries of Moore's law.

Min Ren (S'13–M'14) received the B.S. degree in physics and the Ph.D. degree in optics from East China Normal University, Shanghai, China, in 2005 and 2013, respectively. He is currently a Research Associate in Electrical and Computer Engineering Department, University of Virginia, Charlottesville, VA, USA. His current research interests include photodetectors, avalanche photodiodes, single photon detectors, laser ranging and imaging. He is a member of the IEEE Photonics Society, the Optical Society of America, and SPIE.

Ann-Katheryn Rockwell received the B.S. degree from the University of Alabama, Tuscaloosa, AL, USA, in 2013, and the M.S. degree in electrical engineering in 2016 from the University of Texas at Austin, Austin, TX, USA, where she is currently working toward the Ph.D. degree in electrical engineering. Her current research interests include the design, MBE growth, and characterization of III–V materials for use in low-noise avalanche photodiodes.

Madison E. Woodson received the B.S. degree in biomedical engineering from the University of Virginia, Charlottesville, VA, USA, in 2013, and has since been working toward the Ph.D. degree in the ECE Department. Her research interests include the design, fabrication, and characterization of avalanche photodiodes, particularly for telecommunications applications.

Stephen D. March received the B.S. degree from Iowa State University, Ames, IA, USA, in 2013, and the M.S. degree from the University of Texas at Austin, Austin, TX, USA, in 2016, both in electrical engineering. He is currently working toward the Ph.D. degree at the University of Texas at Austin in electrical engineering. His current research interests include the design, molecular beam epitaxy E growth, and characterization of III–V materials for use in low-noise avalanche photodiodes and photoconductive devices.